Forestry An International Journal of Forest Research

Institute of Chartered Foresters

Forestry 2019; **93**, 38–55, doi:10.1093/forestry/cpz048
Advance Access publication 30 October 2019

Reconstruction of the disturbance history of a temperate coniferous forest through stand-level analysis of airborne LiDAR data

Nuria Sanchez-Lopez[1,*], Luigi Boschetti[1] and Andrew T. Hudak[2]

[1]*University of Idaho, Department of Natural Resources and Society, College of Natural Resources, 875 Perimeter Drive, Moscow, ID 83844, USA*
[2]*US Forest Service (USDA), Rocky Mountain Research Station, RMRS, Forestry Sciences Laboratory, 1221 South Main Street, Moscow, ID 83843, USA*

*Corresponding author: Email: nsanchezlopez@uidaho.edu

Received 4 February 2019

Spatially explicit information about stand-level Time Since the last stand-replacing Disturbance (TSD) is fundamental for modelling many forest ecosystem processes, but most of the current satellite remote sensing mapping approaches are based on change detection and time series analysis, and can detect only disturbances that have occurred since the start of the optical satellite data record. The spatial legacy of stand-replacing disturbances can however persist on the landscape for several decades to centuries, in the form of distinct horizontal and vertical stand structure features. We propose a new approach to reconstruct the long-term disturbance history of a forest, estimating TSD through stand-level analysis of LiDAR data, which are highly sensitive to the three-dimensional forest canopy structure. The study area is in the Nez Perce-Clearwater National Forest in north-central Idaho, where airborne LiDAR covering about 52,000 ha and ancillary TSD reference data for a period of more than 140 years were available. The root mean square difference (RSMD) between predicted and reference TSD was 17.5 years with a BIAS of 0.8 years; and on 72.8% of the stands the predicted TSD was less than 10 years apart from the reference TSD (78.2% of the stands when considering only disturbances occurred in the last 100 years). The results demonstrate that airborne LiDAR-derived data have enough explanatory power to reconstruct the long-term, stand-replacing disturbance history of temperate forested areas at regional scales.

Introduction

Stand-replacing disturbances are a key component of forest ecosystem dynamics (Oliver and Larson, 1996) driving forest structure, function, and composition (Franklin *et al*., 2002; Oliver, 1980). Maps of the long-term disturbance history of a forest would improve estimates of historic, current, and potential carbon sequestration (Bradford *et al*., 2008; Chapin III *et al*., 2002; Pan *et al*., 2011), reduce uncertainties in the carbon budget (Frolking *et al*., 2009), and contribute to a better understanding of disturbance causes and consequences (Cohen *et al*., 2002).

A stand-replacing (major) disturbance is a mortality event (e.g. clearcut, fire, insect outbreak) that frees up growing space and leads to complete replacement of the trees of an entire forest stand, so that post-disturbance regeneration is characterized by competition between a cohort of new trees (Oliver, 1980; Oliver and Larson, 1996). Anthropogenic and natural stand-replacing disturbances result therefore in a patchy and heterogeneous landscape of even-aged forest stands, which are structurally distinct from each other based on their successional state. Long-term stand-replacing disturbance legacies on forested land can persist on the landscape for decades to centuries (Turner, 2010), depending on the forest type. Tree height, canopy density and, more generally, the forest structure are illustrative of these legacies (Spies, 1998), especially in even-aged stands where forest structure is driven by age (Pflugmacher *et al*., 2012).

Traditional approaches to map forest disturbances at regional scales with remotely sensed data have mostly relied on time series analysis of optical data. While single image analysis has limited applications because the persistence of stand-replacing disturbance spectral signatures is limited depending on vegetation recovery rates (Healey *et al*., 2005; Lunetta *et al*., 2004), and the spectral response of vegetation in optical wavelengths saturates in closed canopy forest (Cohen *et al*., 1995; Spanner *et al*., 1990; Turner *et al*., 1999), it is widely established that time series of Earth Observation satellite data can be used to systematically detect forest disturbances at a variety of spatial scales (Cohen and Goward, 2004; Hansen *et al*., 2013). With particular regard to multispectral, moderate resolution data such as those provided by the Landsat satellite series, the detection and characterization of disturbances involves the detection of spectral changes in a time series of observation to detect discontinuities (to capture abrupt events) and/or trends (to capture slower processes) (Hansen *et al*., 2008; Hayes and Sader, 2001; Huang *et al*., 2009; Huo *et al*., 2019; Kennedy *et al*., 2010; Lu *et al*., 2004; Masek *et al*., 2008; Schroeder *et al*., 2011). The main limitation of this approach is that it is necessarily limited to mapping disturbances that have occurred within the temporal extent of the available optical satellite record; at the earliest, 1972 when Landsat-1 was launched with the 60 m resolution Multi-Spectral Scanner (MSS) (e.g. Vogeler *et al*., 2018). The disturbance history of a forest mapped with these approaches, being limited to at most 50 years, is necessarily incomplete in ecosystems where stands may require up to 100 years to mature (Bonnell *et al*., 2011; Fu *et al*., 2017; Liebsch *et al*., 2008). It should also be noted that, while the Landsat archive is largely complete in the United States, in many other parts of the world it is fragmentary until the availability of Landsat-7 in 1999 (Wulder *et al*., 2016).

Approaches for mapping disturbances, on the other hand, have conventionally relied on the pixel as the basic spatial unit of analysis. While pixel-based techniques are computationally faster, the pixel by itself doesn't represent a true geographical feature (Fisher, 1997). Object-based approaches, conversely, use image objects (a discrete region composed by a group of cells internally coherent and different from the surroundings (Blaschke *et al*., 2008)) as the basic spatial unit of analysis. GEOBIA enhances stand-level research since forest stands can be detected as image objects (e.g. Chubey *et al*., 2006; Ke *et al*., 2010; Kim *et al*., 2009; Koch *et al*., 2009; Mallinis *et al*., 2008; Sanchez-Lopez *et al*., 2018; Varo-Martínez *et al*., 2017). Accordingly, it has been used to identify and describe forest disturbances at the stand-level (see Chen *et al*., 2012; Hussain *et al*., 2013). While studies to identify forest disturbances are still mostly multi-temporal, the potential to use object-based analysis on single date datasets to characterize TSD at the stand-level has occasionally been shown in the literature. Wulder *et al*. (2004), for instance, applied object-based analysis to Landsat ETM+ imagery to estimate forest stand age from an approximate time since disturbance to 20 years after harvest. They relied on optical image-derived metrics sensitive to vegetation structure, such as the Tasselled Cap indices, for the predictions, and an object-based analysis to provide a contextual frame of analysis and neglect anomalous cells through different regeneration stages. Their results had an associated estimation error of less than 2.5 years, but the time span of the analysis was relatively small (20 years).

Alternatively, few studies have proposed to use remotely sensed data of the three-dimensional structure of the forest canopy to map forest stand age. Véga and St-Onge (2009), for instance, mapped age and site index of jack pine using known age-height curves and time series of canopy height models derived from aerial photographs. Racine *et al*. (2014) estimated forest age in a managed boreal forest using predictors derived from Light Detection and Ranging (LiDAR) data in 158 field plot locations. This study showed the strong linkage between LiDAR predictor variables, especially LiDAR-derived height, and plot age. In Zhang *et al*. (2014), stand age was mapped across different forest types in China (at 1 km spatial resolution) using biomass estimates derived from canopy height maps (Simard *et al*., 2011). More recently, Vastaranta *et al*. (2016) used time series of image-based digital surface models (DSM) and canopy height models (CHM) to classify forest stand age. All these studies obtained relatively good results, exploiting the strong relationship between forest age and canopy structure. This relationship is particularly significant in the first decades after a stand replacing disturbance, before the height distribution of trees in a mature stand becomes uneven.

In this study, we characterize the stand age of a forest in terms of time since the last stand-replacing disturbance (TSD). We hypothesize that remotely sensed data capturing the three-dimensional structure of the vegetation (i.e. Light Detection and Ranging (LiDAR) is suitable for the long-term estimation of TSD, beyond the timeframe of the available optical remote sensing data record, thus complementing the traditional time-series based TSD mapping approaches. We developed a stand-level, object-based approach to estimate TSD from single-image LiDAR metrics, and we compared the results to independent reference data to assess the accuracy of the prediction.

Materials

Study area

The study area is a temperate mixed-conifer forest located within the Nez Perce-Clearwater National Forest in Idaho (USA), covering 52 257 ha in the Clear Creek, Selway River, and Elk Creek watersheds (Figure 1). Dominant tree species are Douglas-fir (*Pseudotsuga menziesii*) and grand fir (*Abies grandis*), but other species such as western redcedar (*Thuja plicata*) and ponderosa pine (*Pinus ponderosa*) are also common.

The combination of anthropogenic and natural stand-replacing disturbances has generated a patchy landscape of even-aged forest stands. Historical records describe large-scale wildfires happening in this area since the decade of 1870 (Morgan *et al*., 2017; USDA, Forest Service, 2016); of particular relevance are fires occurring in 1919 and 1931 that affected respectively ~12 000 and 3500 ha (i.e., ~23.0 percent and 6.7 percent of the study area). Additionally, timber harvest was common since early in the twentieth century. Logging activity peaked during the 1960s and 1970s, with clearcuts and shelterwoods being the most prevalent harvest practices (Cochrell, 1960; Space, 1964; USDA, Forest Service, 2016).

LiDAR datasets and data pre-processing

Airborne LiDAR data were acquired in 2009 on the Clear Creek watershed and in 2012 on the Selway River and Elk Creek watersheds (Figure 1, Table 1). Point clouds in a binary format (.las) and a digital terrain model (DTM) interpolated from the ground returns at 1-meter spatial resolution were delivered by the provider. The TerraScan software (TerraSolid Ltd, Helsinki, Finland) was used by the vendors to classify ground returns in the point cloud and to interpolate the terrain model. The average pulse density was at least 4 points/m^2 in both flights, and the point cloud was converted to height above ground using the DTM. The LiDAR point cloud was subsequently rasterized, and gridded summary metrics (i.e. statistics summarizing the LiDAR point cloud for a specific cell size) were calculated using the FUSION software (McGaughey, 2009).

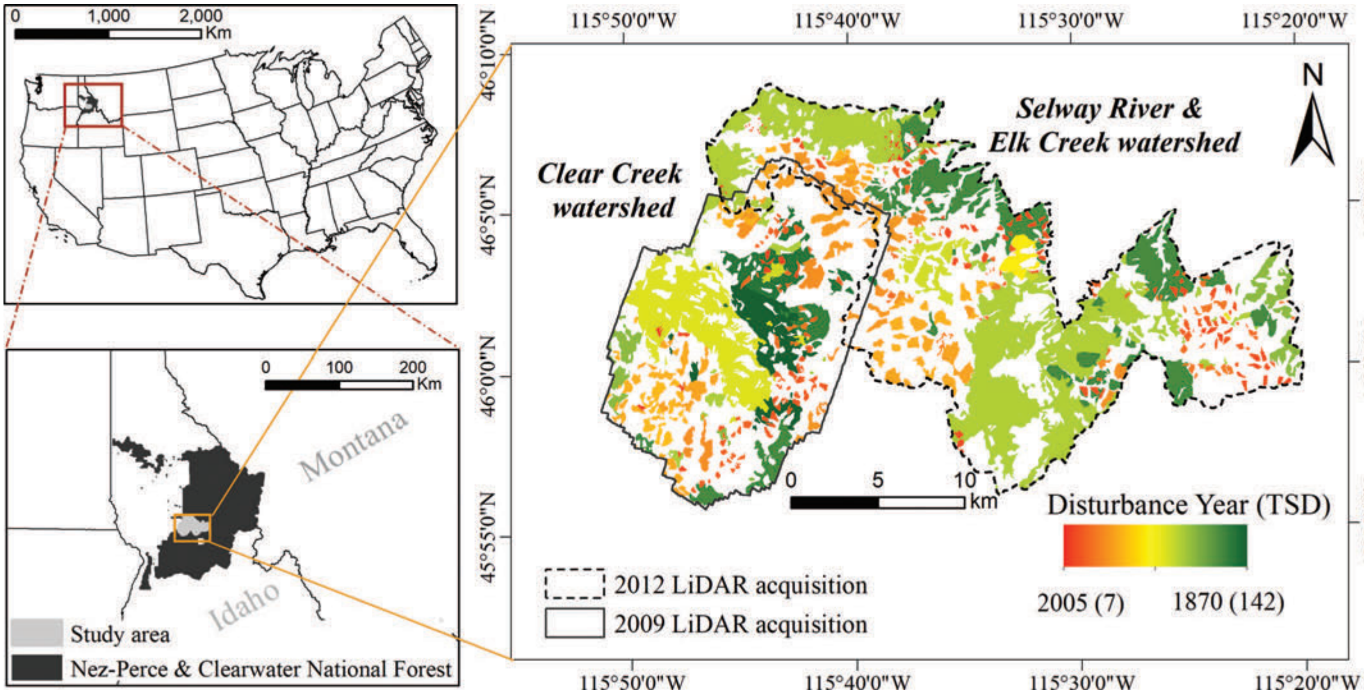

Figure 1 Location of the study area in the Nez Perce-Clearwater National Forest (Idaho, USA); boundaries of the 2009 and 2012 LiDAR acquisitions; ancillary reference dataset of stand-replacing disturbances compiled from historic burns digitized from aerial photos (Morgan *et al*., 2017), and the perimeters of the stand and patch clearcut management units reported in the Forest Service Activity Track System (FACTs) harvest dataset (USDA, Forest Service, 2016). The colour scale indicates the disturbance year (ranging between 2005 and 1870) and Time Since Disturbance (TSD, in parentheses), calculated with reference to 2012, i.e. the year of the more recent LiDAR data acquisition.

Table 1 LiDAR acquisition parameters.

	Clear Creek	Selway River& Elk Creek
Date	October 2009	June–July 2012
vendor	Earth Eye LLC, Orlando, FL	Watershed Sciences, Corvallis, OR
LiDAR sensor	Leica ALS60	Leica ALS50/ALS60 Phase II
Scan angle	±6°	±14°
Pulse rate (Hz)	69 400	88 000
Altitude (m above ground level)	2400–3850	1200–1300
Minimum return density (pts/m^2)	4	4

A total of 21 metrics were generated at 30 m resolution (Table 2): 15 LiDAR canopy metrics (6 related to vegetation canopy height and complexity, and 9 related to canopy density) and 6 topographic metrics. Echoes below 1.37 m above the terrain were ignored to compute vegetation canopy height metrics, assuming that most of them stemmed from ground or understory. If no echoes were found within the 30 m x 30 m grid cell, then that cell was given a value of zero. Canopy height metrics include the average, 5th, 25th, 75th and 95th percentile of the distribution of return height within the cell, and are complemented by the rumple index, which is a measure of canopy complexity. It is defined as the ratio of canopy surface area over the underlying ground surface area (Kane *et al*., 2010; Parker *et al*., 2004) and, unlike the rest of metrics, it was retrieved from a 1-m canopy height model (CHM) and the "GridSurfaceStats" tool within the FUSION software. Canopy density metrics include the percentage of LiDAR returns for different vertical strata of the forest canopy. Additionally, six topographic metrics of elevation, slope, solar radiation index and aspect were derived from the DTM. Aspect in particular is characterized through three transformed metrics: the "SRAI" (Solar-Radiation Aspect Index) is a linear transformation of the topographic aspect (Roberts and Cooper, 1989); the cosine ("SCA") and the sine ("SSA") aspect transformations account for the interaction between aspect and slope, considered of importance for tree growth (Stage, 1976).

The overlap area between the two datasets covers 1271 ha (Figure 1). Since no significant disturbances occurred in the overlap area between the two LiDAR acquisition dates, the cells of the overlapping area were used to assess the mean growth

Table 2 LiDAR derived summary metrics related to canopy structure (height & complexity, and density) and topography, computed as predictor variables for TSD modelling. All metrics are defined in 30 m × 30 m raster cells. On the equations, α is the topographic aspect in degrees

Predictor variables		
Canopy height & complexity	H.Ave	Mean height value
	H05	5th percentile of height above 1.37 m
	H25	25th percentile of height above 1.37 m
	H75	75th percentile of height above 1.37 m
	H95	95th percentile of height above 1.37 m
	Rumple index	Canopy roughness. Canopy complexity
Canopy density	PRT1Mean	Percentage first returns above mean height over first returns
	PRT1BH	Percentage first returns above 1.37 m height over first returns
	ST_b0.15	Percentage of returns below 0.15 m. Inverse of total canopy density
	ST_0.15–1.37	Percentage of returns between 0.15 and 1.37 m
	ST_1.37–5	Percentage of returns between 1.37 and 5 m
	ST_5–10	Percentage of returns between 5 and 10 m
	ST_10–20	Percentage of returns between 10 and 20 m
	ST_20–30	Percentage of returns between 20 and 30 m
	ST_ab30	Percentage of returns above 30 m
Topography	Elevation	Elevation (meters)
	SLP	Slope (percentage)
	SRI	Solar Radiation Index
	SRAI	Topographic solar-radiation aspect index$\mathbf{SRAI} = \frac{1-\cos\left(\left(\frac{\pi}{180}\right)(\alpha-30)\right)}{2}$ (Roberts and Cooper, 1989)
	SCA	Transformation cos (aspect) *x* Percent slopeSCA = SLP x cos(α) (Stage, 1976)
	SSA	Transformation sine (aspect) *x* Percent slopeSCA = SLP x sin(α) (Stage, 1976)

increment between 2009 and 2012 on the canopy height metrics. We then harmonized the height metrics by adding to the 2009 dataset the observed mean growth. Subsequently, the two LiDAR datasets were mosaicked together to obtain a single raster, with metrics nominally reported to 2012, that was used as the reference year in all subsequent steps of the analysis. We note that the mean difference between the two acquisitions was relatively modest (0.07 m, 0.08 m, 0.10 m, 0.03 m, and 0.21 m for “H.Ave”, “H05”, “H25”, “H75” and “H95” respectively) as expected due to the fact that only two complete growing seasons separate the two LiDAR acquisitions (Hopkinson *et al*., 2008; Hudak *et al*., 2012).

Forest stand map

A map of forest stands was used to provide the spatial units of analysis for TSD estimation. It was generated following the object-based strategy presented in Sanchez-Lopez *et al*. (2018) and based on the segmentation of the “H95” metric, identified as the optimal LiDAR metric for the delineation of even-aged forest stands (Sanchez-Lopez *et al*., 2018).

The 30 m raster of the “H95” metric was systematically segmented with different sets of parameters of the multiresolution segmentation (MRS) algorithm (Baatz and Schape, 2000) implemented in eCognition software. Measures of spatial autocorrelation (Böck *et al*., 2017; Espindola *et al*., 2006; Johnson and Xie, 2011) were used to evaluate the resulting set of segmentations, and the segmentation with the maximum degree of intra-segment homogeneity and inter-segment heterogeneity was selected as the optimal stand map. For a complete description of the workflow refer to Sanchez-Lopez *et al*. (2018).

The selected segmentation (i.e. the selected forest stand map) was composed of 1470 image objects (hereafter referred as forest stands) with an average size of 35.6 ha, and median size of 29 ha (Figure 2).

Ancillary reference data and data pre-processing

The FACTS (Forest ACtivity Tracking System) timber harvest dataset (USDA, Forest Service, 2016) was used to locate stand-replacing harvests since 1956. The FACTS dataset is maintained by the U.S. Forest Service and contains polygon features representing forest management units, generally forest stands or forest patches, with an indication of the year in which timber management activities (e.g. clearcut, shelterwood, thinning) were executed. All the stand and patch clearcut management units in the FACTS harvest data record for the study area were initially considered, corresponding to 6200 ha logged between 1956 and 2005. No logging was reported in the area from 2005 to the LiDAR acquisition date.

Additionally, a dataset of burned area perimeters of wildfires from 1870 to 2000 (Morgan *et al*., 2017) was used as a reference dataset for fire disturbance. The burned area perimeters were interpreted by an expert ecologist from fire atlas records and historical aerial photographs when available. The dataset also defines burn severity classes (unburned, low, moderate and high), based on percent of tree mortality of the overstory, visually delineated by the same interpreter within each fire perimeter (Morgan *et al*., 2017). High and moderate severity burns were

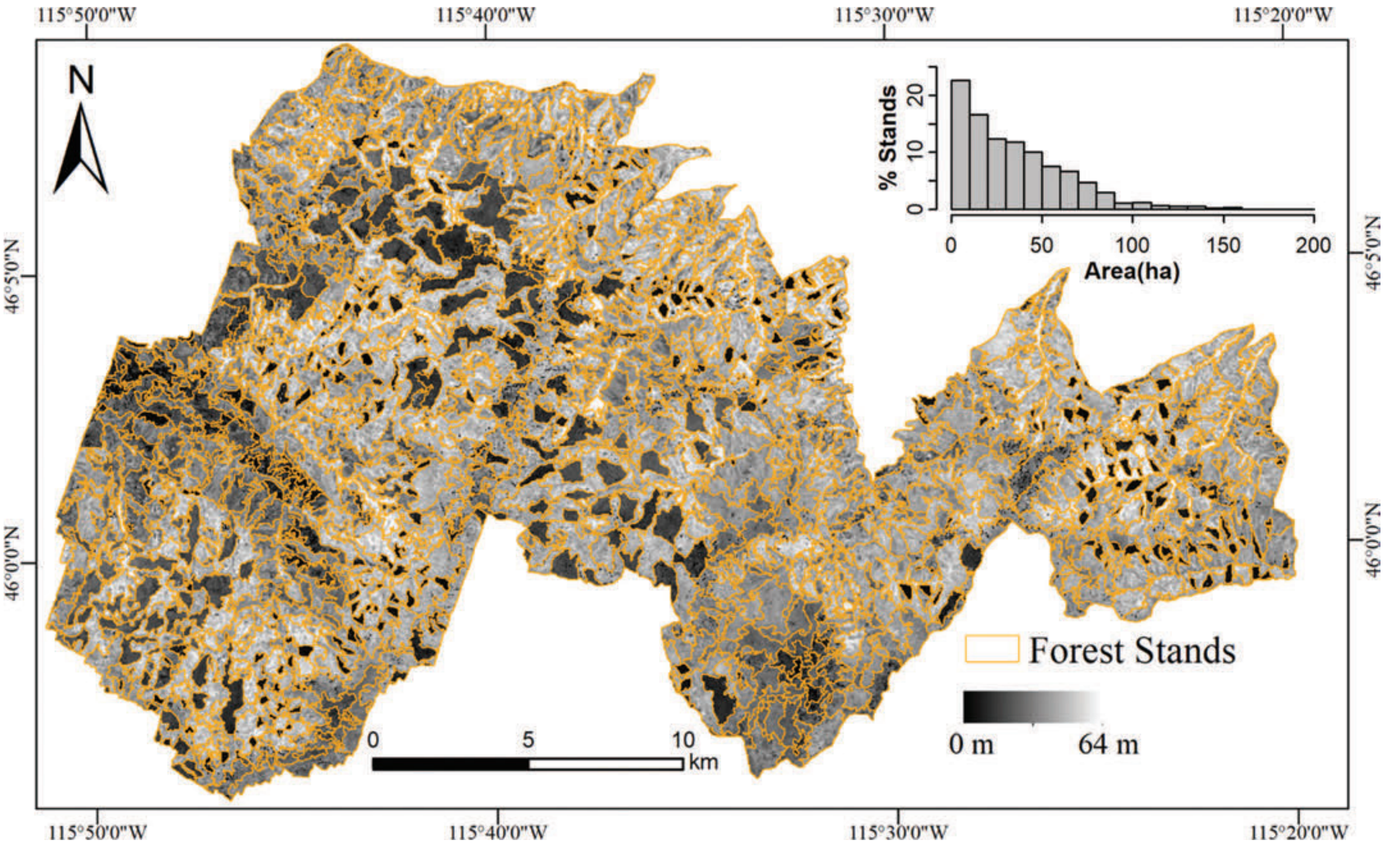

Figure 2 Forest stand map (orange vector) overlaid on the “H95” LiDAR summary metric shown in grayscale. Top-right, histogram showing the percentage distribution of the size of the stands.

considered in our study as stand-replacing disturbance events totaling 22 395 ha, 99.95 percent of which (i.e., ~22 384 ha) were disturbed between 1870 and 1940, and the remaining 0.05 percent (i.e. ~11 ha) were disturbed in 1992.

Time since disturbance (TSD) was computed for all reference data using 2012, i.e. the acquisition date of the second LiDAR dataset, as reference year; consequently, the disturbances present in the reference dataset had TSD ranging from 7 (stands disturbed in 2005) to 142 (stands disturbed in 1870).

The ancillary reference dataset assembled from the FACTs harvests and the historical burns was manually refined: post-disturbances (i.e. small areas with evident biomass removal or other post-logging activity, especially within the fire perimeters) and bare ground areas were manually digitized through visual interpretation of the 2011 National Agricultural Imagery Program (NAIP) imagery (1 m spatial resolution) and the LiDAR data, then erased from the compiled disturbance reference dataset. Additionally, three polygons reported as clearcuts in the 1950s were removed from the dataset since no evidence of actual harvest could be observed. Neighboring forest management units harvested in consecutive years showed small differences in their structure due to low growth of vegetation during consecutive cuts and were considered as part of the same forest stand. Thus, following the procedure introduced in Sanchez-Lopez *et al*. (2018), units sharing borders and harvested within a short time interval (≤5 years) were merged as exemplified in Figure 3, top row. The year of harvest assigned to each aggregated forest stand was calculated as the weighted average of the merged management units accounting for the relative area of each of the integrating stands. Figure 1 shows the location and TSD of the stand-replacing disturbances, compiled from the FACTS dataset and the burned area perimeters, and pre-processed as described above.

Further pre-processing was needed to match the ancillary dataset with the forest stand map. As exemplified in Figure 3, bottom row, there is a degree of mismatching between the perimeters of the ancillary reference dataset and the forest stand perimeters, due to the different processing methodologies (i.e. photointerpretation for the reference datasets, semiautomatic image segmentation for the stand map) and data sources (historical records and aerial photographs for the reference datasets, LiDAR for the stand map). To reconcile the two datasets, we defined as “Forest stands with known TSD” the segmented forest stands whose area overlapped by at least 50 percent with the area of the ancillary reference data polygons defined above. The 50 percent area criterion is commonly used in the GEOBIA literature for matching objects across datasets (Clinton *et al*., 2010; Drăguţ *et al*., 2014; Liu *et al*., 2012; Zhan *et al*., 2005). The histogram of the overlapping area between the forest stands and the ancillary dataset (Figure 4) shows that there is generally a good agreement between the two datasets: only 26 percent of the forest overlap less than 75 percent with the

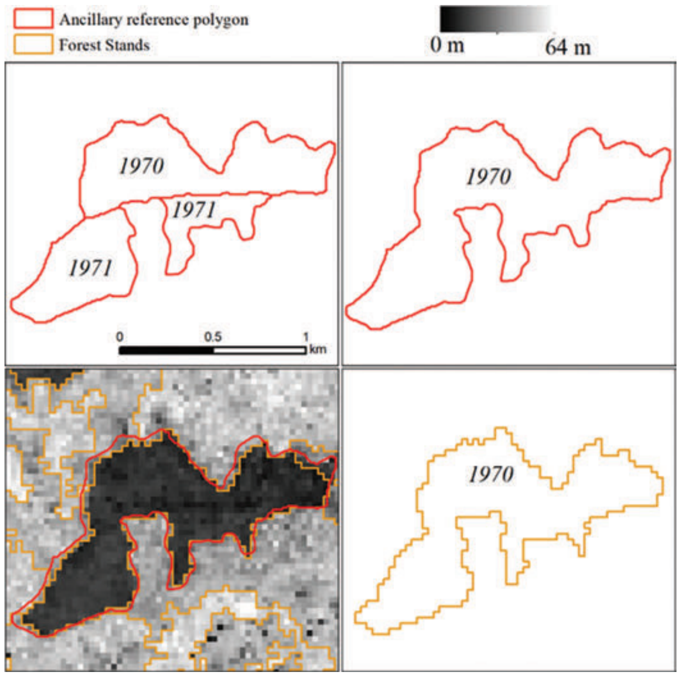

Figure 3 Pre-processing of the FACTs harvest management units (top row) and selection of forest stands with known TSD (bottom row). The top row shows an example of adjacent polygons harvested within a time interval ≤ 5 years (left) that are merged into aggregated polygons (right) that are used as ancillary reference polygons. Bottom row shows the corresponding forest stand with known TSD selected from the forest stand map (Figure 2) according to the 50 percent overlap area criterion. The "H95" LiDAR summary metric is shown in grayscale in the bottom left figure.

reference dataset, and among these, 78 percent correspond to old fires.

Additionally, 50 undisturbed forest stands, covering a total area of 2121 ha, were visually identified overlaying the 1-meter spatial resolution NAIP imagery, the rasterized LiDAR metrics (Table 2), and the ancillary reference dataset. These forest stands were mainly characterized by high height of the dominant cohort of the forest canopy, for instance, the mean "H95" was 43.7 m, while the mean "H95" of the stands disturbed in 1870 and 1880 was 36.3 and 34.1 m respectively. Thus, they were considered non-disturbed since 1870 (i.e. TSD greater than 142 years) and were added to the reference dataset, to ensure that it represented all the stand types within the study area.

Figure 4 shows the 781 (731 disturbed and 50 non-disturbed) forest stands (26 644 ha) which, hereafter, are all considered forest stands with known TSD, and Table 3 summarizes accordingly the disturbed area by decade of both the ancillary reference dataset and the forest stands with known TSD.

Methods

A disturbance history map was obtained using a Random Forest (RF) classifier (Breiman, 2001) to impute TSD over a period of 142 years. The methodology involved five main steps (Figure 5): (1) training stand data selection following a LiDAR-assisted stratification strategy; (2) TSD estimation; first, at the cell-level imputing TSD from RF with LiDAR metrics as predictor variables; and second, at the stand-level using the perimeters of the stands to calculate median TSD from the cell-level imputations; (3) accuracy assessment using the stands with known TSD as reference (Figure 4); (4) analysis of the predictor variable importance; and (5) sensitivity analysis of the stratification strategy and the sample size of the training data.

Training dataset

A training set of stands with known TSD (Figure 4) was extracted through stratified random sampling. A stratification based on topography ("SRAI") and canopy height ("H95") was used to ensure the representativeness of the training set. Previous studies have demonstrated that LiDAR-assisted plot stratification of LiDAR-based forest inventories is cost-effective to reduce the number of field plots required for model calibration compared to simple random sampling (Gobakken *et al*., 2013; Hawbaker *et al*., 2009).

The transformed solar-radiation aspect index ("SRAI", Table 2), was selected as the first metric. "SRAI" ranges between 0 and 1, where areas with values close to 0 are north-northeast oriented, i.e. cooler and moistier; and areas with values close to 1 are south-shouthwest oriented, i.e. warmer and drier. Considering the strong linkage between canopy height and age (Racine *et al*., 2014), the choice was made to have one of the height metrics as the second stratification metric. To select the metric among the five canopy height metrics listed in Table 2, Pairwise Pearson correlations coefficients (R) were calculated between TSD and mean value of each canopy metric based on all the stands with known TSD (i.e. the stands reported in Figure 4). The "H95" metric resulted in highest correlation ($R = 0.89$) and was selected as the second stratification metric.

A hierarchical, two level stratification approach was used. Two "SRAI" strata (high "SRAI"/low "SRAI") of equal size were defined, using the median of the stand-level SRAI as threshold. Within each "SRAI" stratum, five "H95" canopy height strata (based on the mean "H95" per stand) were defined, using the quintiles of the "H95" distribution. As a result, ten strata of equal size were identified (Figure 6).

The training dataset was selected by extracting randomly five forest stands from each of the 10 strata (50 stands). Additionally, the three forest stands with the lowest and the three forest stands with highest "H95" (i.e. 6 forest stands) were added to the training dataset to ensure that the full dynamic range of canopy heights was represented, which is particularly relevant for using RF classifiers since decision trees cannot effectively extrapolate results out of the range of the training dataset (Zimmerman *et al*., 2018). The resulting training dataset included 56 stands, as reported in Figure 6.

TSD estimation

A stand-level map of estimated TSD was obtained in two steps. First, TSD for each 30 m raster cell was imputed through the RF; TSD at the stand-level was subsequently obtained as the

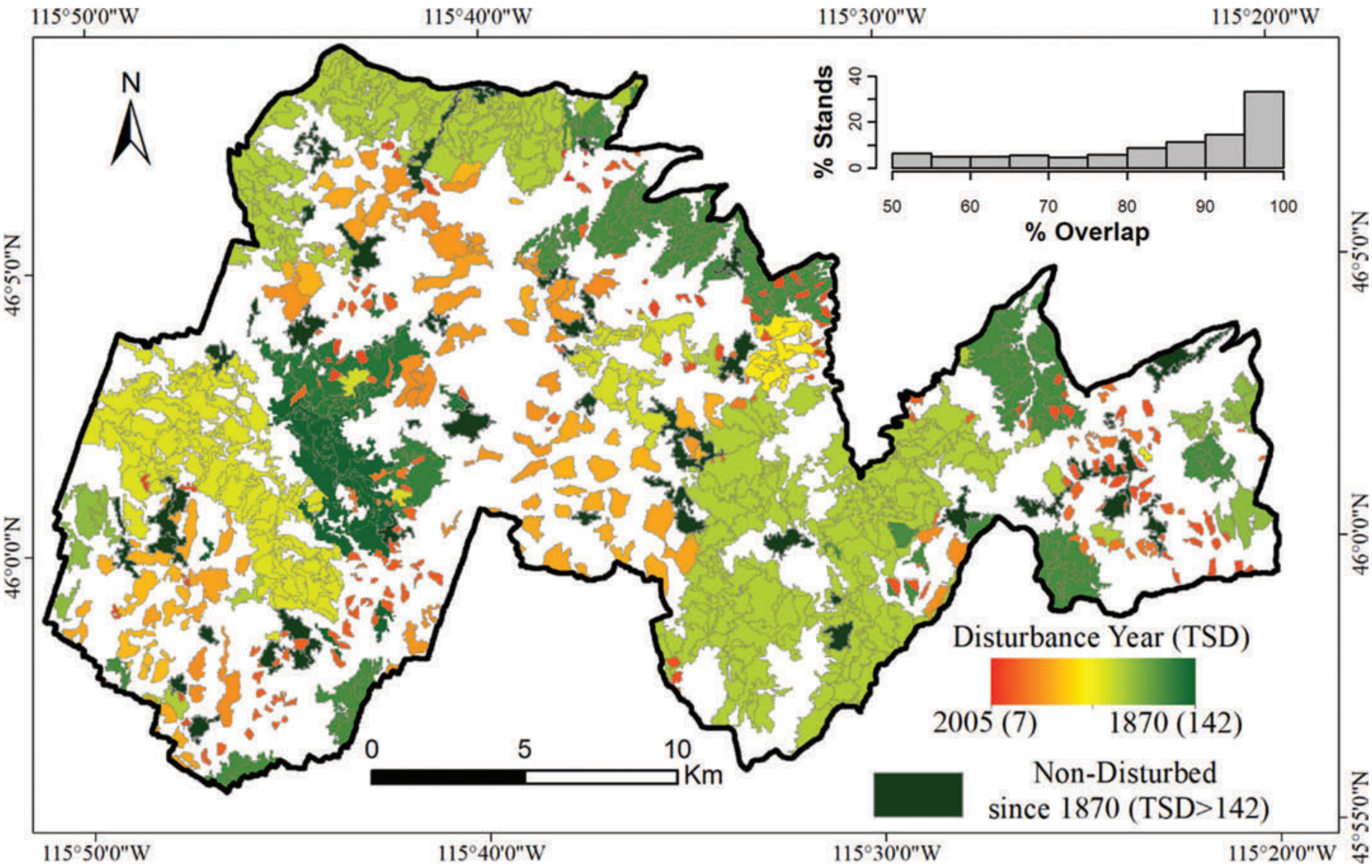

Figure 4 Forest stands with known TSD. Colour ramp indicates the disturbance year (ranging between 2005 and 1870) and Time Since Disturbance (TSD). Top-right, histogram showing the percentage distribution of the overlapping area (in %) between the forest stands with known TSD and the ancillary reference dataset (Figure 1).

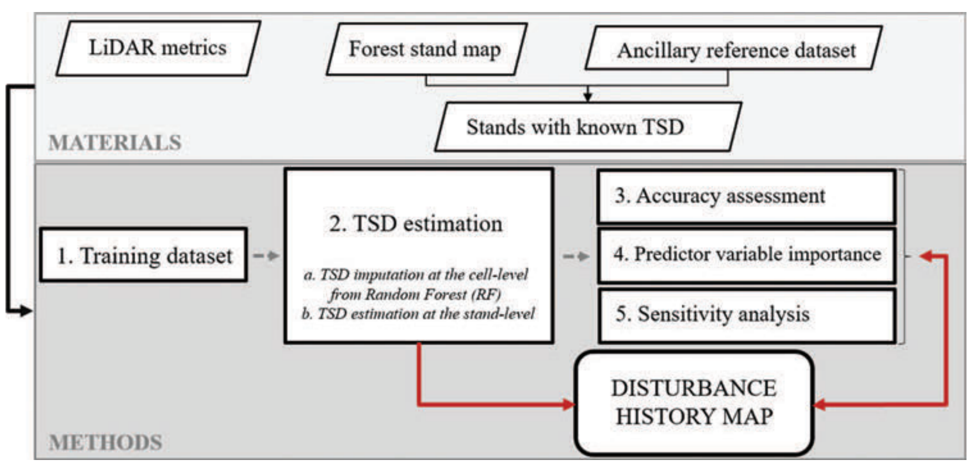

Figure 5 Workflow of the proposed methodology to generate a map of estimated Time Since the last stand-replacing Disturbance (TSD) at the forest stand-level.

median value of the cell-level imputations within each forest stand (Figure 2).

The raster cells within the 56 training forest stands were used to train the RF classifier; the TSD as determined by the reference dataset was used as the dependent (response) variable, and all the LiDAR metrics as independent (predictor) variables. RF is relatively insensitive to outliers and data noise, but errors in the predictions might increase exponentially if a 20 percent noise threshold is reached (Rodriguez-Galiano *et al*., 2012). Consequently, outliers were removed from the training data by

Table 3 Disturbed area reported on the ancillary reference dataset (Figure 1) and on the selected forest stands with known TSD (Figure 4) summarized by decade. Area is reported in number of disturbed hectares, and in percentage relative to the extent of the entire study area (52 257 ha). ND: forest stands non-disturbed since 1870.

	Ancillary reference dataset		Forest Stands with known TSD	
Disturbance Decade	Area (ha)	Relative area (%)	Area (ha)	Relative area (%)
ND	-	-	2121	4.06
1870	1199	2.29	1031	1.97
1880	5509	10.54	4745	9.08
1890	0	0.00	0	0.00
1900	0	0.00	0	0.00
1910	9928	19.00	9718	18.60
1920	756	1.45	644	1.23
1930	2884	5.52	2845	5.44
1940	278	0.53	322	0.62
1950	102	0.20	75	0.14
1960	2415	4.62	2176	4.16
1970	1799	3.44	1584	3.03
1980	773	1.48	614	1.18
1990	1026	1.96	758	1.45
2000	57	0.11	13	0.02
Total	26 725	51.1	26 644	51.0

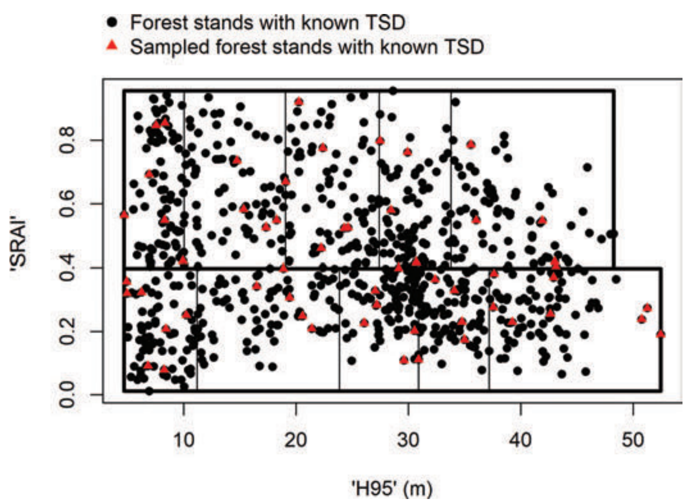

Figure 6 Scheme of the LiDAR-assisted stratification of the forest stands with known TSD. The mean topographic solar-radiation aspect index ("SRAI") and the mean 95th percentile of height above 1.37 m ("H95") are used as stratification variables. The 56 stands used as training dataset are reported as red triangles.

removing the individual cells with "H95" below the 5th or above the 95th percentiles of the distribution of each stand. Outliers in the study area are primarily due to old stands where the uneven-aged distribution of the canopy is reached and the likelihood to encounter gaps with young trees due to tree mortality increases (Runkle, 1982). Other problematic areas include recently harvested stands where some old standing trees, not representative of TSD, are left for seedling and cells at the edge of the stands in cases where there is a significant border effect.

The 56 training objects identified a total of 17 604 cell observations used to train the RF model. These cells represented ~1584 ha, i.e. 3.0 percent of the study area. Disturbances were unequally distributed over time (Table 3, Figure 1) as reflected in the number of training stands per disturbance decade (Table 4).

The *yai* function implemented on the *yaImpute* R package (Crookston and Finley, 2008) was used to train the RF classifier. The number of decision trees was set at 500 and the number of LiDAR variables available to split at each tree node at the default value, i.e. as the square root of the number of predictor variables. The Out-of-Bag (OOB) error estimate of the RF was calculated. As defined here, RF randomly sampled two thirds of the available training observations to build each of the 500 decision trees. A predicted error is then obtained using the defined tree on the Out-Of-Bag (i.e. non-included) portion of the training data. The average of the predicted errors of all the trees is the OOB error estimate.

The AsciiGridImpute function on the yaImpute R package was used to impute TSD at the raster cell-level over the whole study area; and TSD at the stand-level was then calculated as the median of all the TSD cell values enclosed within the perimeters of each forest stand.

Accuracy assessment

The forest stands with known TSD (Figure 4) and not used to train the RF were used as reference data to assess the accuracy of the TSD stand predictions. The forest stands visually identified as non-disturbed (i.e. 44 stands since 6 were part of the training set) were similarly excluded from the validation dataset since the actual age of the last stand-replacing disturbance was unknown.

Table 4 Number and percentage of stands with known TSD within the study area summarized by decade; and number and percentage of sampled forest stands following the LiDAR-assisted stratification strategy (Figure 6). ND: forest stands non-disturbed since 1870

Decade	# Stands with known TSD	Stand with known TSD (%)	# Sampled stands	Sampled stands (%)
ND	50	6	6	11
1870	23	3	2	4
1880	112	14	7	13
1890	0	0	0	0
1900	0	0	0	0
1910	202	26	12	21
1920	14	2	0	0
1930	72	9	8	14
1940	11	1	1	2
1950	5	1	0	0
1960	57	7	6	11
1970	46	6	1	2
1980	89	11	3	5
1990	96	12	9	16
2000	4	1	1	2

As a result, the accuracy assessment was conducted on a total of 681 stands.

The accuracy of the predictions at the forest stand-level was evaluated using five metrics, defined as follows.

Root Mean Square Difference between predicted and observed TSD (RMSD):

$$\mathrm{RMSD} = \sqrt{\frac{\sum_{i=1}^{n}\left(\hat{Y}_i - Y_i\right)^2}{n}} \tag{1}$$

where n is the number of forest stands, $\hat{Y}_i$ is the predicted TSD for stand i, and Y_i is the observed TSD for stand i. RMSD has been used in imputation as an accuracy metric similar to the traditional RMSE used for regression model accuracy (Stage and Crookston, 2007).

Relative RMSD ($\mathbf{RMSD}_{rel}$):

$$\mathrm{RMSD}_{rel} = \frac{\mathrm{RMSD}}{\frac{1}{n}\sum_{i=1}^{n} Y_i} \times 100 \tag{2}$$

where n is the number of forest stands, and Y_i is the observed TSD for stand i.

The bias (BIAS):

$$BIAS = \frac{1}{n}\sum_{i=1}^{n}\left(\hat{Y}_i - Y_i\right) \tag{3}$$

where n is the number of forest stands, $\hat{Y}_i$ is the predicted TSD for stand i, and Y_i is the observed TSD for stand i. The bias shows overall trend in over and underestimations between predicted and observed year of disturbance.

Relative bias ($\mathbf{BIAS}_{rel}$):

$$\mathrm{BIAS}_{rel} = \frac{\sum_{i=1}^{n}\left(\hat{Y}_i - Y_i\right)}{\sum_{i=1}^{n} Y_i} \times 100 \tag{4}$$

where n is the number of forest stands, $\hat{Y}_i$ is the predicted TSD for stand i, and Y_i is the observed TSD for stand i.

Percentage of forest stands that had less than 10 years of absolute error (Perct.10):

$$Perct.10 = \left(\frac{\sum_{i=1}^{n}\left|\hat{Y}_i - Y_i\right| < 10}{n}\right) \times 100 \tag{5}$$

where n is the number of forest stands, $\hat{Y}_i$ is the predicted TSD for stand i, and Y_i is the observed TSD for stand i.

Additionally, a confusion matrix of the stand-level predictions aggregated by decade was also computed, using the reference dataset as defined above, with the addition of the 44 undisturbed forest stands not used in the training.

Predictor variable importance.

Because there is significant correlation among the predictor metrics of each group (i.e. canopy height & complexity, canopy density, topography), the measures of variable importance that are directly generated by RF classifiers can potentially result in spurious rankings that do not reflect the actual importance of the predictors (Nicodemus *et al*., 2010; Strobl *et al*., 2008). The relative importance of the predictor variables was therefore assessed though the methods proposed by Roy and Kumar (2017) and Tulbure *et al*. (2012). The method was specifically designed to deal with correlated predictor variables.

We examined all the possible combinations of predictor metrics selecting one metric at a time from each of the three groups,

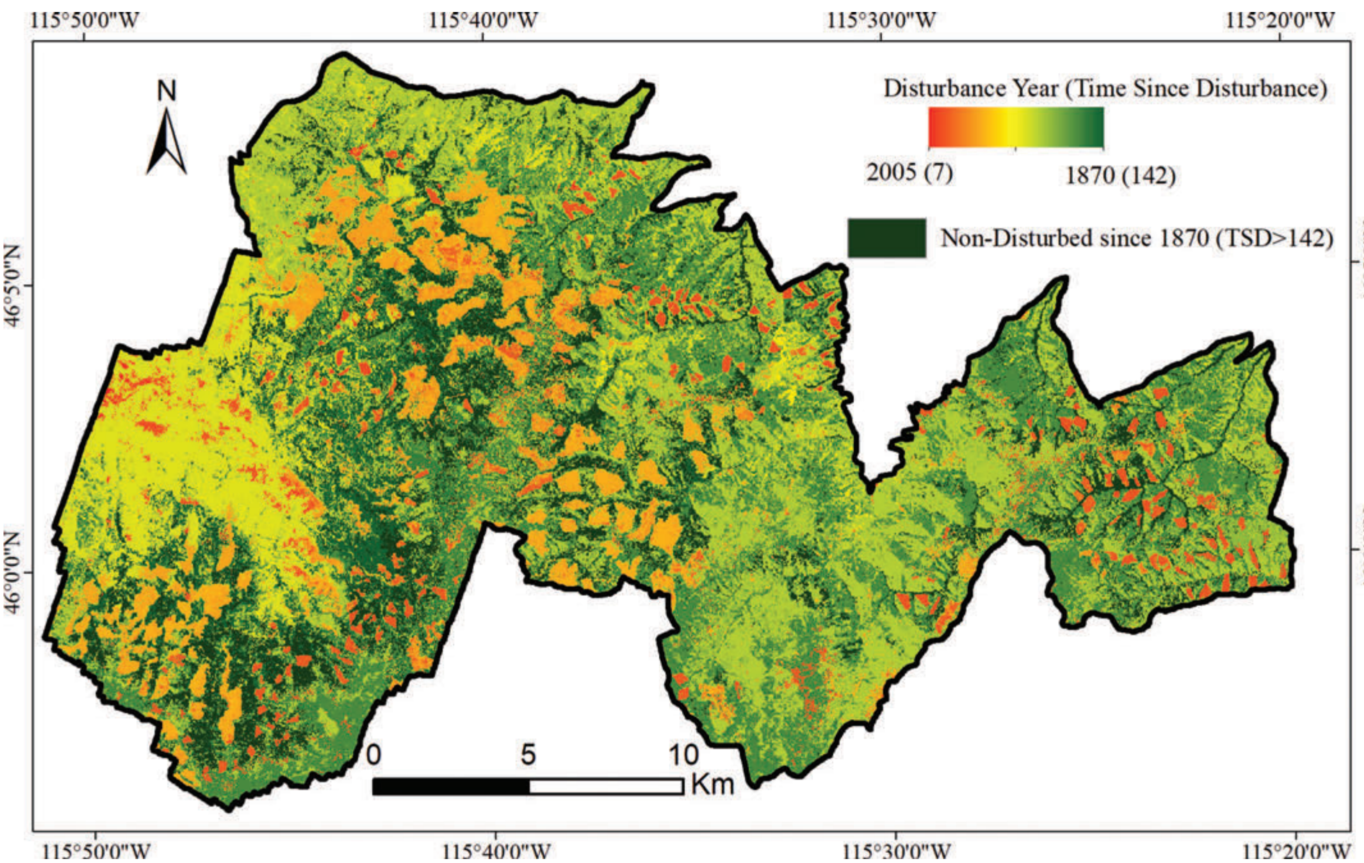

Figure 7 TSD imputations at the cell level using RF analysis and 21 LiDAR predictor variables related to canopy structure and topography (Table 2).

resulting in a total of 324 combinations. If the predictor metrics of a particular combination were highly correlated (i.e. absolute value |R| of the Pearson coefficient greater than 0.5), then the combination was discarded. For each uncorrelated combination, a RF classifier was trained and the Mean Decrease in the Gini (MDG) index, which is a robust metric of variable importance (Breiman, 2001), was used to rank the three predictors. The percentage of times that each specific metric ranked first, second and third was calculated, and used as overall measure of the relative importance of each predictor and group.

Additionally, partial dependence plots with probability distribution based on scaled margin distances of the most important metrics were generated using the rf.partial.prob function implemented in the R rfUtilities package (Evans and Murphy, 2018).

Sensitivity analysis

A sensitivity analysis was performed, to determine the sensitivity of the accuracy metrics to the sample size. The number of randomly selected forest stands in each stratum was varied from 1 to 10, and for each size the random selection was repeated 10 times. The three forest stands with the lowest and the highest "H95" (i.e. 6 forest stands) were always included in the training dataset. The entire classification procedure was repeated for each set (100 output classifications in total), and the accuracy of each classification was assessed by computing the RMSD, BIAS and Perct.10 metrics. Non-parametric statistics (median, 25th and 75th percentiles) of the accuracy metrics were calculated for each sample size.

Results

TSD estimation

The RF classifier was trained using the 17 604 cells selected as detailed above, and cell-level imputations of TSD were generated for the entire study area (Figure 7). The OOB (Out of Bag) error estimate of the RF is considered as a robust indicator of error rate that correlates well with the estimated error of cross-validation and it was relatively low (OOB error = 0.10).

The cell level TSD imputations were subsequently aggregated through the use of the median operator to generate the stand-level disturbance history map, displayed in Figure 8. The study area was broadly disturbed by fires in 1919, so this historic disturbance event was well represented in the training data (Table 4), in the cell-level imputation (Figure 7), and in the disturbance history map (Figure 8).

Accuracy assessment

RMSD was 17.5 years and $\mathbf{RMSD}_{rel}$ was 24.2 percent, while BIAS was 0.8 years and $\mathbf{BIAS}_{rel}$ was 1.1 percent, i.e. the predicted year

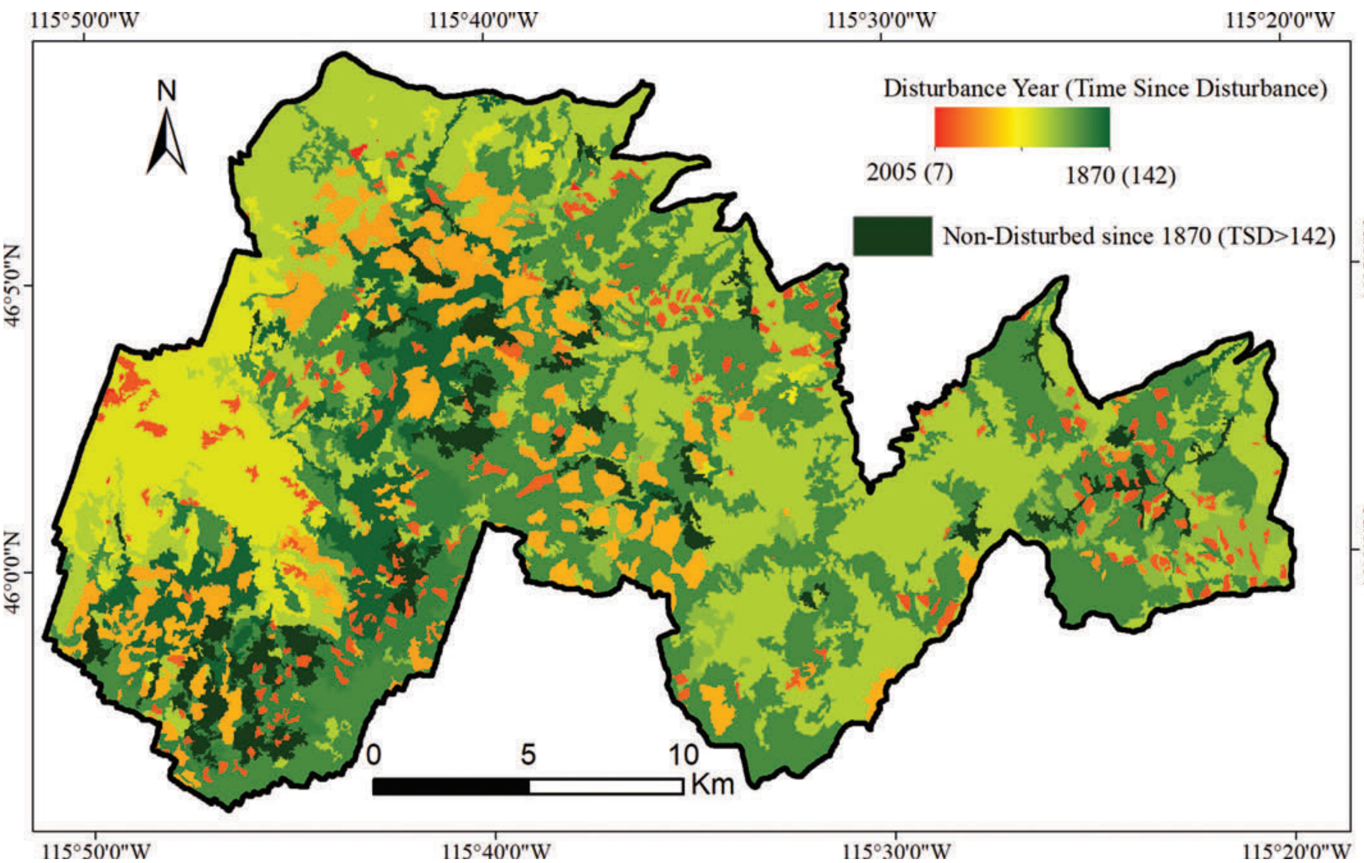

Figure 8 Stand-replacing disturbance history map. TSD stand-level calculated as the median value of the imputed TSD (Figure 7) cell estimates enclosed within the perimeters of the forest stands (Figure 2).

of the disturbance was slightly before to the observed year. The percentage of stands with less than 10 years of absolute error (Perct.10) was relatively high (77.8 percent.) considering the large dataset of forest stands included in the accuracy assessment; i.e. 681 stands after excluding the 56 stands selected for training and the 44 non-disturbed stands (Figure 4); this percentage increased to 78.4 percent when only stands disturbed since the decade of 1910 were considered (i.e. forest stands disturbed within the last 100 years).

The confusion matrix of the disturbance history map at decadal steps (Table 5) showed a relatively good agreement between reference and predicted TSD values, especially in recently disturbed stands (i.e. forest stands disturbed within the last 60 years) where confusion mainly happened between subsequent decades. On the other hand, forest stands disturbed in the 1930s (specifically in 1931) were sometimes classified as disturbed in the 1910s (specifically in 1919); and forest stands disturbed in the 1880s were often classified as disturbed in the 1910s and vice versa.

Predictor variable importance

Table 6 presents the results of the variable importance analysis. Out of the 324 possible combinations of predictor metrics from each group (Table 2), 210 had low pairwise correlation between metrics (i.e. $|R| < 0.5$) and were retained in the analysis. Significant correlation between Canopy density and Canopy height & complexity metrics was observed: for example, the "ST_ab30" and the "ST_5–10" density metrics had high correlation with all canopy height and complexity metrics—rumple index excepted—and were therefore only included in six combinations. Topography metrics were always uncorrelated with the metrics from the other two groups.

The "H95" metric had the highest predictive power among all metrics: every time it was in a combination, it ranked first in importance based on MDG. It was followed by "H.Ave", "H75" and the Rumple index, all ranking first 83 percent of the times. When the results are aggregated by group (Table 7), the Canopy height & complexity group are the most important (ranking first in 82 percent of the combinations), followed by the topography (13 percent) and density metrics (5 percent).

The partial dependence plots (Figure 9) of the four most important metrics indicate that recent disturbances are characterized by less variability of the LiDAR metrics compared to older disturbances. The mode of the probability distribution of each of the curves of the "H95", "H.Ave" and "H75" metrics for each TSD class (aggregated in 10-year bins) also shows a general pattern of monotonic relationship between tree height and TSD. Among the variables, "H95" shows a better ability to discriminate TSD than the other two height metrics. For instance, considering

Table 5 Confusion matrix of the TSD stand-level estimates of the 725 forest stands with known TSD not used to train the RF (Table 4) summarized by decade. In bold, forest stands correctly classified. ND: forest stands non-disturbed since 1870

	Reference data															
Predictions	*ND*	*1870*	*1880*	*1890*	*1900*	*1910*	*1920*	*1930*	*1940*	*1950*	*1960*	*1970*	*1980*	*1990*	*2000*	*Total*
ND	**22**	*0*	*1*	*0*	*0*	*0*	*0*	*0*	*0*	*0*	*0*	*0*	*0*	*0*	*0*	*23*
1870	8	**8**	4	0	0	0	0	0	0	0	0	0	0	0	0	20
1880	12	7	**53**	0	0	31	1	1	1	0	0	0	0	1	0	107
1890	0	0	0	**0**	0	0	0	0	0	0	0	0	0	0	0	0
1900	0	0	0	0	**0**	0	0	0	0	0	0	0	0	0	0	0
1910	2	5	45	0	0	**148**	12	10	6	0	1	3	0	1	0	233
1920	0	0	0	0	0	0	**0**	0	0	0	0	0	0	0	0	0
1930	0	1	1	0	0	8	1	**47**	3	1	6	3	3	1	2	77
1940	0	0	0	0	0	0	0	0	**0**	0	0	0	0	0	0	0
1950	0	0	0	0	0	0	0	0	0	**0**	0	0	0	0	0	0
1960	0	0	1	0	0	2	0	5	0	4	**44**	31	11	1	0	99
1970	0	0	0	0	0	0	0	0	0	0	0	**3**	4	0	0	7
1980	0	0	0	0	0	0	0	0	0	0	0	5	**39**	11	0	55
1990	0	0	0	0	0	1	0	1	0	0	0	0	29	**72**	0	103
2000	*0*	*0*	*0*	*0*	*0*	*0*	*0*	*0*	*0*	*0*	*0*	*0*	*0*	*0*	***1***	*1*
Total	44	21	105	0	0	190	14	64	10	5	51	45	86	87	3	***725***

Table 6 Percentage and number (in brackets) of times that a predictor variable included in uncorrelated variable combinations ranked 1st, 2nd, or 3rd in order of importance based on the Mean Decrease in Gini (MDG) index of the RF. In bold, metric ranking first in importance. Pearson correlation threshold $|R| = 0.5$ for uncorrelated variable combination

Predictor variable		Rank		
		1	2	3
Canopy height & complexity	H.Ave	83% (20)	17% (4)	0% (0)
	H05	69% (25)	28% (10)	3% (1)
	H25	63% (15)	33% (8)	4% (1)
	H75	83% (25)	17% (5)	0% (0)
	H95	**100% (42)**	0% (0)	0% (0)
	Rumple index	83% (45)	17% (9)	0% (0)
Canopy density	PRT1Mean	0% (0)	17% (2)	83% (10)
	PRT1BH	0% (0)	13% (13)	88% (21)
	ST_b0.15	0% (0)	25% (9)	75% (27)
	ST_0.15–1.37	0% (0)	0% (0)	100% (36)
	ST_1.37–5	0% (0)	05 (0)	100% (36)
	ST_5–10	0% (0)	83% (5)	17% (1)
	ST_10–20	0% (0)	445 (8)	56% (10)
	ST_20–30	28% (10)	61% (22)	11% (4)
	ST_ab30	0% (0)	83% (5)	17% (1)
Topography	Elevation	80% (28)	20% (7)	0% (0)
	SLP	0% (0)	71% (25)	29% (10)
	SRI	0% (0)	77% (27)	23% (8)
	SCA	0% (0)	77% (27)	23% (8)
	SSA	0% (0)	60% (21)	40% (14)
	TRSI	0% (0)	37% (13)	63% (22)

the “H95” metric, the mode of the probability distribution for the 10–19 years TSD class corresponds to a height of ~4.5 m, and it increases to ~10.5 m for the 20–29 years TSD class. By contrast, “H75” and “H.Ave” are less sensitive to TSD: the mode of the 10–19 year TSD class is ~3 m for “H75” and ~2 m for “H.Ave, and the mode of the 20-29 year TSD class is ~4 m for ‘H75” and ~3 m for ‘H.Ave. The rumple index, which is a measure of canopy complexity, shows that the complexity of the canopy increases

Table 7 Relative predictor variable importance summarized by group of metrics (Table 2), showing the percentage (and number) of uncorrelated variable combinations (out 210) that a variable from a group ranked 1st, 2nd, or 3rd (rank one is the most important) according to the Mean Decrease in Gini (MDG) index of the RF

	Rank		
Predictor variable group	1	2	3
Canopy height & complexity	82% (172)	17% (36)	1% (2)
Canopy density	5% (10)	26% (54)	69% (146)
Topography	13% (28)	57% (120)	30% (62)

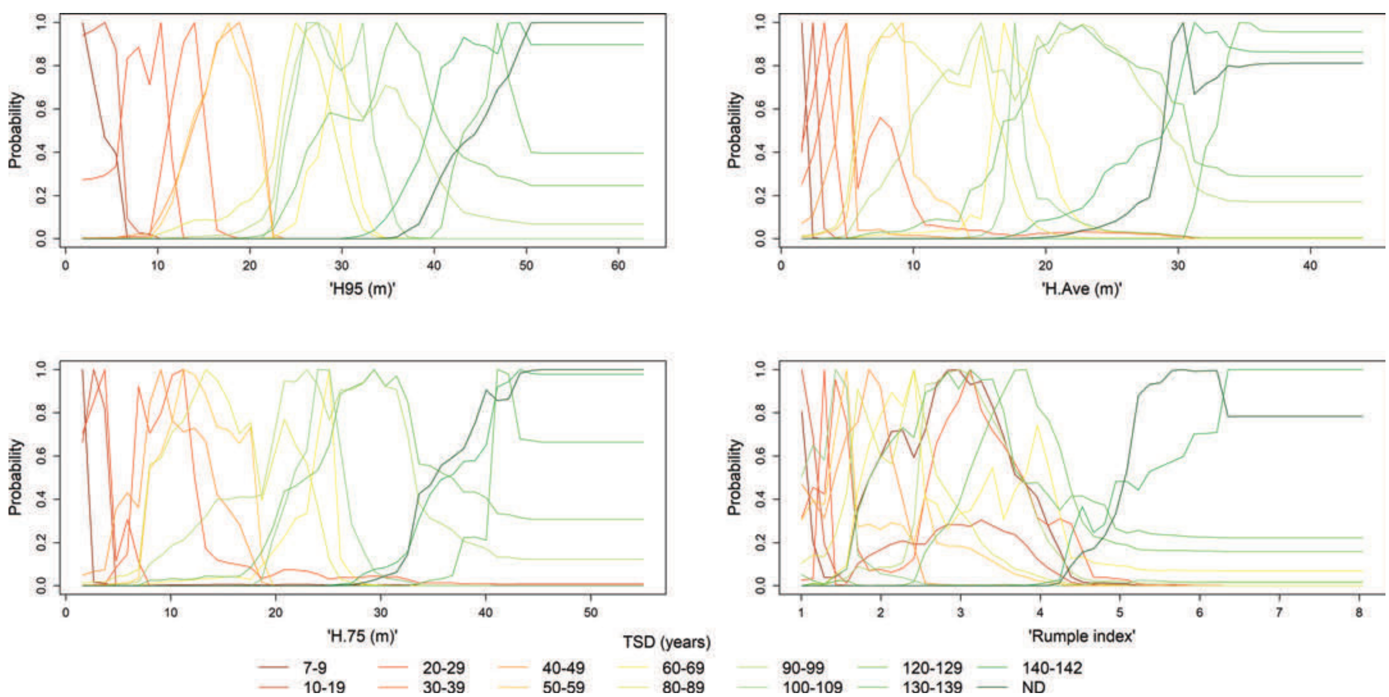

Figure 9 Partial dependence plots with probability distribution of TSD for the four variables with the highest importance (Table 6). Each curve represents the conditional TSD probability as a function of the LiDAR metrics (TSD is aggregated in 10-year bins).

with stand age, albeit without a clear separation, except for the separation between the oldest stands, and those disturbed in the last 140 years.

Sensitivity analysis

One hundred disturbance history maps were obtained varying the number of forest stands selected per stratum in the stratification (from 1 to 10) (Figure 5), and replicating the random selection as well 10 times.

Overall accuracy was influenced by the number of training stands, with the highest accuracy achieved when ten stands are selected and dropping very significantly especially when fewer than four stands per stratum were selected (Figure 10). RMSD ranged from 20.0 to 32.2 years (median: 24.6 years) if only one forest stand was sampled; it ranged from 17.4 to 21.3 years (median: 19.6 years) if five stands were sampled; and from 15.4 to 19.2 years (median: 17.5 years) if ten stands were sampled. Similarly, BIAS ranged from −1.3 to 18.8 years (median: 4.8 years) if only one stand was sampled; it ranged from −0.8 to 6.6 years (median: 2.1 years) if five stands were sampled; and from −1.9 and 2.3 years (median: −0.9 years) if ten stands were sampled. And finally, Perct.10 ranged from 41.9 and 65.3 percent (median: 51.8 percent) if one stand was sampled, it ranged from 64.2 to 72.8 percent (median: 70.8 percent) if five stands were sampled, and from 70.2 to 80.1 percent (median: 74.5 percent) if ten stands were sampled.

Discussion

TSD is generally missing or incomplete for most forested areas and rarely extends to the past longer than the available satellite record. Traditionally, field data collection can expand such record, but this requires time-consuming and expensive field inventory and dendrochronological analyses (Speer, 2010).

This study presents a methodology to predict TSD and map disturbances at the stand-level using RF analysis on single date

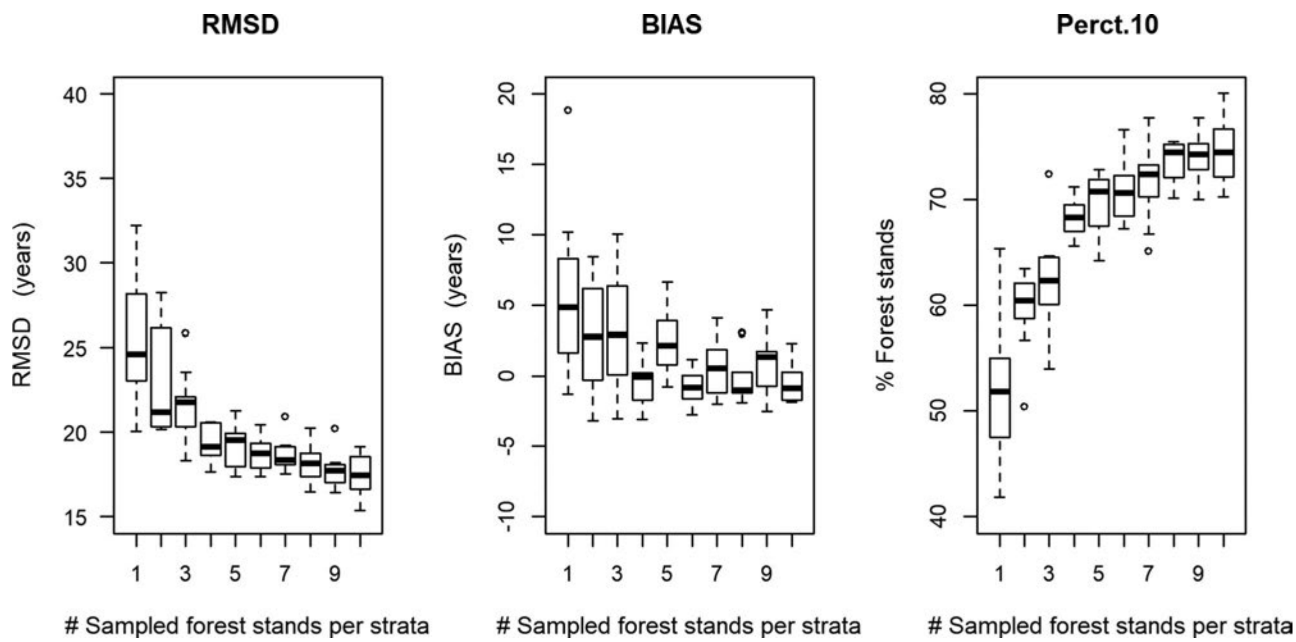

Figure 10 Boxplots of RMSD, BIAS, and Perct.10 obtained for TSD predictions when 1 to 10 forest stands were selected per stratum (Figure 6). The random selection of forest stands was replicated 10 times. Central line represents the median, edges of the box are the first (i.e. the 25th percentile) and the third (i.e. 75th percentile) quartiles, and the whiskers are 1.5 times the range of the upper and lower quartiles.

airborne LiDAR data. This approach is designed to complement the more established optical-data based methodologies used for detecting forest disturbances, which are limited by the temporal coverage of the optical Earth Observation record. Our results indicate that canopy LiDAR metrics are well suited to reconstruct the long term disturbance history of a forest, provided that reference data of the different disturbance times is available for training a RF imputation. Additionally, the introduction of meaningful spatial units of analysis (i.e. even-aged forest stands) introduces contextual information that is advantageous to reduce the time required for analysis (i.e. by reducing the amount of training data required to impute TSD); and to reduce the inherent variability of cell-level analyses. This is particularly relevant when estimating an attribute—such as TSD—that is inherently constant across all cells of a stand. Another methodological advantage, apart from above comments on the stand-level approach, is the use of current, single-date LiDAR data, which reduces the amount of historical time series data required to impute TSD. The disturbance history map obtained by applying the proposed methodology shows good accuracy, as reflected by the overall RMSD (17.5 years), BIAS (0.08 years) and Perct.10 (72.8 percent). Unsurprisingly, the progressively uneven-aged distribution of the canopy due to natural tree mortality of pioneer species creating gaps that become filled with younger trees (Luyssaert *et al.*, 2008) negatively affects the overall accuracy of the TSD estimation for very old disturbances (>100 years).

The predictor variable importance analysis indicated that canopy height metrics are the strongest TSD predictors, followed by topography and by density. This is not surprising considering the well-known, strong relationship between stand age and growth (Monserud, 1984; Oliver and Larson, 1996; Ryan *et al.*, 2004). The "H95" metric, in particular, had the highest importance, reflecting the fact that it represents the dominant cohort of the forest canopy (Kane *et al.*, 2010). It was hence expected to have a stronger predictive power than other percentiles of the return height distribution. Our variable importance ranking is consistent with previously published results: Racine *et al.* (2014) predicted stand age on field plots using similar LiDAR predictors as used in the present research, and K-NN imputation, finding "H95" to be the most important predictor of stand age, and the topographic elevation the most significant out of the topographic metrics included in their research as site index indicators. Out of the density metrics used in our study, the "ST_20_30" metric was the most important 28 percent of the times and ranked second 61 percent of the times, which might be explained because in many stands 20–30 m is the range encompassing the height of the dominant tree cohort, as reflected by the distribution of "H95" in the stands with known TSD (the mean "H95" is 24.5 m, the median "H95" is 26.1 m, see Figure 6). The density metrics might therefore capture some residual variability of the structural complexity of the landscape, and consequently contribute to the TSD prediction.

The uncertainties of the TSD prediction, reflected by the accuracy metrics, can be attributed, at least in part, to the uncertainties of the ancillary reference dataset: any errors in the reference data would translate into inaccuracies both in the TSD imputation and in the accuracy assessment. Although theoretically the TSD ancillary dataset covered the study area wall-to-wall, and extended for 140 years of past disturbances, the record is not complete. Harvest reference data prior to the 1950s are missing, and false negatives are likely present in the burn history dataset. The areas located within the perimeters of the 1919 and the 1931 large fires, for instance, were very heterogeneous in vegetation structure parameters, and it is likely that some post-fire logging had occurred before the start of the FACTS data record. In these cases, the site conditions and the actual severity of the fires in each specific stand drives the recovery rates at different phases, making one decade between two disturbance events not enough to substantially distinguish the successional states of some stands (e.g. there are only twelve years of difference between the large fires of 1919 and 1931). Therefore, some confusion in the classification was expected, especially in old stands (Table 5). Misclassification in these cases was also accentuated by the scarcity or outrights absence of reference data in some specific decades (e.g. 1900, 1890) and the overrepresentation of other decades (e.g. 1910s).

These limitations notwithstanding, this study showed that it is possible to generate a classification of TSD with high accuracy at the decadal scale by using only 56 forest stands as training dataset, i.e. 3.8 percent of the total number of stands of the study area. The sensitivity analysis indicates that the accuracy of the methodology has low sensitivity to the size of the training set, with the accuracy of the TSD prediction dropping significantly only when fewer than four stands are selected from each stratum (Figure 10). This is a particularly significant result, because it indicates that a limited amount of fieldwork would be sufficient to generate enough training data to apply the proposed methodology to a new area where no reference data are available. Furthermore, the stratification is entirely based on topographic and LiDAR metrics, hence not requiring any prior knowledge of the TSD distribution.

We demonstrated that forest structure as observed by LiDAR is a strong predictor for stand-level TSD in the area considered by this study. This complements recent studies that have implemented LiDAR to characterize the recovery of vegetation (up to 25 years of TSD) in boreal forest after stand-replacing disturbances (e.g, Bolton *et al*., 2015; White *et al*., 2018). However, some caution should be used when extrapolating these results to different ecosystems. The good performance of the proposed methodology might be influenced by the particular conditions of the study area, covering a temperate mixed-conifer forest subject to high disturbance pressure, with more than half of the study area having undergone stand-replacing disturbances since 1870 (Table 3). While other management activities such as occasional overstory removal, salvage cuts, and biomass removal have been accomplished in the study area (USDA, Forest Service, 2016), even-aged management (including clearcut, shelterwood and seed-tree harvest) was the dominant regeneration method. The landscape is therefore dominated by even-aged forest stands of relatively large size (average of 35.5 ha), which are the result of large wildfires that occurred at the beginning of the 20th century and widespread harvest in the second half of the 20th century. In other areas of the world, the mosaics created by even-aged management might be less evident if the stands are smaller, and uneven-aged and intermediate cutting are predominantly. Similarly, fire disturbance regimes in other ecoregions might determine other landscape structural shapes depending on the predominant severity and extension of the burns. Besides this, stand development and recovery rates after a disturbance also depend on the geographic location (Cole *et al*., 2014), pre-disturbance situation (Ilisson and Chen, 2009) which can determine atypical stand structures, and post-disturbance management. In the former case, for instance, burnt biomass removal is rare in large forests such as those of the Pacific Northwest, especially in areas hard to reach, while it is a more common practice in European countries with more accessible areas. Other management practices, such as planting, accelerate vegetation regeneration rates compared to natural regrowth, which is a slower process since trees regenerate over several decades (Pregitzer and Euskirchen, 2004). As a result, accurate TSD prediction in different ecoregions and forest types might require a different stratification strategy and a larger training dataset than in the present study.

Conclusions

The disturbance history map obtained in this research largely expands the temporal contextualization of stand-replacing disturbances beyond what can be done with traditional optical remotely sensed data and change detection analysis. Stand-replacing disturbance legacies in the Nez Perce-Clearwater National forest remain distinct in the horizontal and vertical structures of the vegetation for a long period (i.e. ∼100 years), and LiDAR canopy and topographic metrics have enough explanatory power to categorize these disturbance patterns through time. The obtained map is unprecedented in the literature considering both the temporal extent (>140 years) and the approach (stand-level based) of the analysis, and its overall accuracy is satisfactory especially within the first 100 years after disturbance occurrence, requiring a relatively low amount of training stands to generate it. On the other hand, the integration of meaningful spatial units of analysis in the workflow (i.e. forest stand perimeters) provides a contextual frame of analysis that constitutes a methodological advantage to improve TSD estimates, among other reasons, because information of the spatial relationship between cells gets intrinsically incorporated into the analysis.

We expect stand-replacing disturbance legacies in the form of horizontal and vertical canopy structural signatures to be recognizable with LiDAR data for a long period in temperate forests with similar disturbance dynamics (e.g. other forests in the Pacific Northwest). Therefore, LiDAR data can be used to map disturbances that pre-date the beginning of the Landsat data record in 1972 and have potential to model disturbance patterns over the long-term (i.e., ∼100 years), implementing a stand-level analysis.

Overall, the combination of different data sources and strategies to reconstruct the disturbance history of forested areas, including this methodology, will increase the amount of reliable ready-to-use maps of TSD, which are required to improve carbon cycle modelling and the understanding of forest ecosystem processes. Further research would involve the replication of the analysis to other study sites, the evaluation of other predictors to impute TSD, such as climatic variables, and the categorization of other disturbance attributes such as typology or severity.

Acknowledgements

We thank Pat Green and Penny Morgan for sharing the portion of the historic fire geodatabase that overlapped the FACTS geodatabase and

LiDAR acquisitions to delimit our study area. A field campaign (not related to the present paper) was conducted in the study area in 2016. It greatly contributed to design this research, therefore, we thank to everyone who helped on it, especially to Darko Veljković, Patrick Fekety, Patrick Mahoney and Adrienne Marshall. We also thank two anonymous reviewers and the editors of this journal for their comments on an earlier version of this manuscript.

Conflict of interest statement

The authors declare no conflict of interest.

Funding

The project is supported by NASA's Land-Cover/Land-Use Change (LCLUC) program (award number NHX14AD92G) and the Carbon Monitoring System (CMS) (award number NNH15AZ06I); and by the United States Department of Agriculture (USDA) under award USDA NIFA 2011-32100-06016

References

Baatz, M. and Schape, A. 2000 Multiresolution segmentation–an optimization approach for high quality multi-scale image segmentation. *AGIT-Symposium Salzburg* **2000**, 12–23.

Blaschke, T., Lang, S. and Hay, G. 2008 *Object-Based Image Analysis: Spatial Concepts for Knowledge-Driven Remote Sensing Applications*, Springer Science & Business Media.

Böck, S., Immitzer, M. and Atzberger, C. 2017 On the objectivity of the objective function—Problems with unsupervised segmentation evaluation based on global score and a possible remedy. *Remote Sens.* **9**, 769.

Bolton, D.K., Coops, N.C. and Wulder, M.A. 2015 Characterizing residual structure and forest recovery following high-severity fire in the western boreal of Canada using Landsat time-series and airborne lidar data. *Remote Sens. Environ.* **163**, 48–60.

Bonnell, T.R., Reyna-Hurtado, R. and Chapman, C.A. 2011 Post-logging recovery time is longer than expected in an east African tropical forest. *For. Ecol. Manag.* **261**, 855–864.

Bradford, J.B., Birdsey, R.A., Joyce, L.A. and Ryan, M.G. 2008 Tree age, disturbance history, and carbon stocks and fluxes in subalpine Rocky Mountain forests. *Glob. Change Biol.* **14**, 2882–2897.

Breiman, L. 2001 Random forests. *Mach. Learn.* **45**, 5–32.

Chapin, F.S. III, Matson, P.A. and Mooney, H.A. 2002 *Principles of terrestrial ecosystem ecology*. springer-Verlag, N. Y. USA, pp. 298–300.

Chen, G., Hay, G.J., Carvalho, L.M. and Wulder, M.A. 2012 Object-based change detection. *Int. J. Remote Sens.* **33**, 4434–4457.

Chubey, M.S., Franklin, S.E. and Wulder, M.A. 2006 Object-based analysis of Ikonos-2 imagery for extraction of Forest inventory parameters. *Photogramm. Eng. Remote Sens.* **72**, 383–394.

Clinton, N., Holt, A., Scarborough, J., Yan, L.I. and Gong, P. 2010 Accuracy assessment measures for object-based image segmentation goodness. *Photogramm. Eng. Remote Sens.* **76**, 289–299.

Cochrell, A.N. 1960 *The Nezperce Story: A History of the Nezperce National Forest*. USDA Forest Service, Missoula, MT, USA.

Cohen, W.B. and Goward, S.N. 2004 Landsat's role in ecological applications of remote sensing. *BioScience* **54**, 535–545 (2004)054[0535:LRIEAO]2.0.CO;2.

Cohen, W.B., Spies, T.A., Alig, R.J., Oetter, D.R., Maiersperger, T.K. and Fiorella, M. 2002 Characterizing 23 years (1972–95) of stand replacement disturbance in western Oregon forests with Landsat imagery. *Ecosystems* **5**, 122–137.

Cohen, W.B., Spies, T.A. and Fiorella, M. 1995 Estimating the age and structure of forests in a multi-ownership landscape of western Oregon, U.S.a. Int. J. *Remote Sens.* **16**, 721–746.

Cole, L.E., Bhagwat, S.A. and Willis, K.J. 2014 Recovery and resilience of tropical forests after disturbance. *Nat. Commun.* **5**, 3906.

Crooskton, N.L. and Finley, A.O. 2008 yaImpute: an R package for kNN imputation. *J. Stat. Softw.* **23(**10**)**, 16.

Drăguţ, L., Csillik, O., Eisank, C. and Tiede, D. 2014 Automated parameterisation for multi-scale image segmentation on multiple layers. *ISPRS J. Photogramm. Remote Sens.* **88**, 119–127.

Espindola, G.M., Camara, G., Reis, I.A., Bins, L.S. and Monteiro, A.M. 2006 Parameter selection for region-growing image segmentation algorithms using spatial autocorrelation. *Int. J. Remote Sens.* **27**, 3035–3040.

Evans, J.S., Murphy, M.A. 2018. Package 'rfUtilities.' R package version 2.1–4.

Fisher, P. 1997 The pixel: A snare and a delusion. *Int. J. Remote Sens.* **18**, 679–685.

Franklin, J.F., Spies, T.A., Pelt, R.V., Carey, A.B., Thornburgh, D.A., Berg, D.R., Lindenmayer, D.B., Harmon, M.E., Keeton, W.S., Shaw, D.C., Bible, K. and Chen, J. 2002 Disturbances and structural development of natural forest ecosystems with silvicultural implications, using Douglas-fir forests as an example. For. Ecol. Manag. *Forest Ecology in the next Millennium: Putting the long view into Practice* **155**, 399–423 (01)00575-8.

Frolking, S., Palace, M.W., Clark, D.B., Chambers, J.Q., Shugart, H.H. and Hurtt, G.C. 2009 Forest disturbance and recovery: A general review in the context of spaceborne remote sensing of impacts on aboveground biomass and canopy structure. *J. Geophys. Res. Biogeosciences* **114**, G00E02.

Fu, Z., Li, D., Hararuk, O., Schwalm, C., Luo, Y., Yan, L. and Niu, S. 2017 Recovery time and state change of terrestrial carbon cycle after disturbance. *Environ. Res. Lett.* **12**, 104004.

Gobakken, T., Korhonen, L. and N\a esset, E. 2013 Laser-assisted selection of field plots for an area-based forest inventory. *Silva Fenn.* **47**, 943.

Hansen, M.C., Potapov, P.V., Moore, R., Hancher, M., Turubanova, S.A., Tyukavina, A., Thau, D., Stehman, S.V., Goetz, S.J., Loveland, T.R., Kommareddy, A., Egorov, A., Chini, L., Justice, C.O. and Townshend, J.R.G. 2013 High-resolution global maps of 21st-century Forest cover change. *Science* **342**, 850–853.

Hansen, M.C., Stehman, S.V., Potapov, P.V., Loveland, T.R., Townshend, J.R.G., DeFries, R.S., Pittman, K.W., Arunarwati, B., Stolle, F., Steininger, M.K., Carroll, M. and DiMiceli, C. 2008 Humid tropical forest clearing from 2000 to 2005 quantified by using multitemporal and multiresolution remotely sensed data. *Proc. Natl. Acad. Sci.* **105**, 9439–9444.

Hawbaker, T.J., Keuler, N.S., Lesak, A.A., Gobakken, T., Contrucci, K. and Radeloff, V.C. 2009 Improved estimates of forest vegetation structure and biomass with a LiDAR-optimized sampling design. *J. Geophys. Res. Biogeosciences* **114**, G00E04.

Hayes, D.J. and Sader, S.A. 2001 Comparison of change-detection techniques for monitoring tropical forest clearing and vegetation regrowth in a time series. *Photogramm. Eng. Remote Sens.* **67**, 1067–1075.

Healey, S.P., Cohen, W.B., Zhiqiang, Y. and Krankina, O.N. 2005 Comparison of tasseled cap-based Landsat data structures for use in forest disturbance detection. *Remote Sens. Environ.* **97**, 301–310.

Hopkinson, C., Chasmer, L. and Hall, R.J. 2008 The uncertainty in conifer plantation growth prediction from multi-temporal lidar datasets. *Remote Sens. Environ.* **112**, 1168–1180.

Huang, C., Goward, S.N., Masek, J.G., Gao, F., Vermote, E.F., Thomas, N., Schleeweis, K., Kennedy, R.E., Zhu, Z., Eidenshink, J.C. and Townshend, J.R.G. 2009 Development of time series stacks of Landsat images for reconstructing forest disturbance history. *Int. J. Digit. Earth* **2**, 195–218.

Hudak, A.T., Strand, E.K., Vierling, L.A., Byrne, J.C., Eitel, J.U.H., Martinuzzi, S. and Falkowski, M.J. 2012 Quantifying aboveground forest carbon pools and fluxes from repeat LiDAR surveys. *Remote Sens. Environ.* **123**, 25–40.

Huo, L.-Z., Boschetti, L. and Sparks, A.M. 2019 Object-based classification of Forest disturbance types in the conterminous United States. *Remote Sens.* **11**, 477.

Hussain, M., Chen, D., Cheng, A., Wei, H. and Stanley, D. 2013 Change detection from remotely sensed images: From pixel-based to object-based approaches. *ISPRS J. Photogramm. Remote Sens.* **80**, 91–106.

Ilisson, T. and Chen, H.Y. 2009 Response of six boreal tree species to stand replacing fire and clearcutting. *Ecosystems* **12**, 820–829.

Johnson, B. and Xie, Z. 2011 Unsupervised image segmentation evaluation and refinement using a multi-scale approach. *ISPRS J. Photogramm. Remote Sens.* **66**, 473–483.

Kane, V.R., McGaughey, R.J., Bakker, J.D., Gersonde, R.F., Lutz, J.A. and Franklin, J.F. 2010 Comparisons between field- and LiDAR-based measures of stand structural complexity. *Can. J. For. Res.* **40**, 761–773.

Ke, Y., Quackenbush, L.J. and Im, J. 2010 Synergistic use of QuickBird multispectral imagery and LIDAR data for object-based forest species classification. *Remote Sens. Environ.* **114**, 1141–1154.

Kennedy, R.E., Yang, Z. and Cohen, W.B. 2010 Detecting trends in forest disturbance and recovery using yearly Landsat time series: 1. LandTrendr — Temporal segmentation algorithms. *Remote Sens. Environ.* **114**, 2897–2910.

Kim, M., Madden, M. and Warner, T.A. 2009 Forest type mapping using object-specific texture measures from multispectral Ikonos imagery. *Photogramm. Eng. Remote Sens.* **75**, 819–829.

Koch, B., Straub, C., Dees, M., Wang, Y. and Weinacker, H. 2009 Airborne laser data for stand delineation and information extraction. *Int. J. Remote Sens.* **30**, 935–963.

Liebsch, D., Marques, M.C. and Goldenberg, R. 2008 How long does the Atlantic rain Forest take to recover after a disturbance? Changes in species composition and ecological features during secondary succession. *Biol. Conserv.* **141**, 1717–1725.

Liu, Y., Bian, L., Meng, Y., Wang, H., Zhang, S., Yang, Y., Shao, X. and Wang, B. 2012 Discrepancy measures for selecting optimal combination of parameter values in object-based image analysis. *ISPRS J. Photogramm. Remote Sens.* **68**, 144–156.

Lu, D., Mausel, P., Brondízio, E. and Moran, E. 2004 Change detection techniques. *Int. J. Remote Sens.* **25**, 2365–2401.

Lunetta, R.S., Johnson, D.M., Lyon, J.G. and Crotwell, J. 2004 Impacts of imagery temporal frequency on land-cover change detection monitoring. *Remote Sens. Environ.* **89**, 444–454.

Luyssaert, S., Schulze, E.-D., Börner, A., Knohl, A., Hessenmöller, D., Law, B.E., Ciais, P. and Grace, J. 2008 Old-growth forests as global carbon sinks. *Nature* **455**, 213–215.

Mallinis, G., Koutsias, N., Tsakiri-Strati, M. and Karteris, M. 2008 Object-based classification using Quickbird imagery for delineating forest vegetation polygons in a Mediterranean test site. *ISPRS J. Photogramm. Remote Sens.* **63**, 237–250.

Masek, J.G., Huang, C., Wolfe, R., Cohen, W., Hall, F., Kutler, J. and Nelson, P. 2008 North American forest disturbance mapped from a decadal Landsat record. *Remote Sens. Environ.* **112**, 2914–2926.

McGaughey, R.J. 2009 FUSION/LDV: Software for LIDAR data analysis and visualization. US Department of Agriculture, Forest Service, Pacific Northwest Research Station.

Monserud, R.A. 1984 Height growth and site index curves for inland Douglas-fir based on stem analysis data and Forest habitat type. *For. Sci.* **30**, 943–965.

Morgan, P., Hudak, A.T., Wells, A., Parks, S.A., Baggett, L.S., Bright, B.C. and Green, P. 2017 Multidecadal trends in area burned with high severity in the Selway-bitterroot wilderness area 1880–2012. *Int. J. Wildland Fire* **26**, 930–943.

Nicodemus, K.K., Malley, J.D., Strobl, C. and Ziegler, A. 2010 The behaviour of random forest permutation-based variable importance measures under predictor correlation. *BMC Bioinformatics* **11**, 110.

Oliver, C.D. 1980 Forest development in North America following major disturbances. *For. Ecol. Manag.* **3**, 153–168.

Oliver, C.D. and Larson, B.C. 1996 *Forest stand dynamics: updated edition*. John Wiley and sons.

Pan, Y., Chen, J.M., Birdsey, R., McCullough, K., He, L. and Deng, F. 2011 Age structure and disturbance legacy of north American forests. *Biogeosciences* **8**, 715–732.

Parker, G.G., Harmon, M.E., Lefsky, M.A., Chen, J., Van Pelt, R., Weis, S.B., Thomas, S.C., Winner, W.E., Shaw, D.C. and Frankling, J.F. 2004 Three-dimensional structure of an old-growth Pseudotsuga-Tsuga canopy and its implications for radiation balance, microclimate, and gas exchange. *Ecosystems* **7**, 440–453.

Pflugmacher, D., Cohen, W.B. and Kennedy, E. 2012 Using Landsat-derived disturbance history (1972–2010) to predict current forest structure. Remote Sens. Environ. *Landsat Legacy Special Issue* **122**, 146–165.

Pregitzer, K.S. and Euskirchen, E.S. 2004 Carbon cycling and storage in world forests: Biome patterns related to forest age. *Glob. Change Biol.* **10**, 2052–2077.

Racine, E.B., Coops, N.C., St-Onge, B. and Bégin, J. 2014 Estimating Forest stand age from LiDAR-derived predictors and nearest neighbor imputation. *For. Sci.* **60**, 128–136.

Roberts, D.W.U.S.U. and Cooper, S.V. 1989 Concepts and techniques of vegetation mapping. Gen. Tech. Rep. INT - US Dep. Agric. For. Serv. Intermt. Res. Stn. USA.

Rodriguez-Galiano, V.F., Chica-Olmo, M., Abarca-Hernandez, F., Atkinson, P.M. and Jeganathan, C. 2012 Random Forest classification of Mediterranean land cover using multi-seasonal imagery and multi-seasonal texture. *Remote Sens. Environ.* **121**, 93–107.

Roy, D.P. and Kumar, S.S. 2017 Multi-year MODIS active fire type classification over the Brazilian tropical moist Forest biome. *Int. J. Digit. Earth* **10**, 54–84.

Runkle, J.R. 1982 Patterns of disturbance in some old-growth Mesic forests of eastern North America. *Ecology* **63**, 1533–1546.

Ryan, M.G., Binkley, D., Fownes, J.H., Giardina, C.P. and Senock, R.S. 2004 An experimental test of the causes of Forest growth decline with stand age. *Ecol. Monogr.* **74**, 393–414.

Sanchez-Lopez, N., Boschetti, L. and Hudak, A. 2018 Semi-automated delineation of stands in an even-age dominated Forest: A LiDAR-GEOBIA two-Stage evaluation strategy. *Remote Sens.* **10**, 1622.

Schroeder, T.A., Wulder, M.A., Healey, S.P. and Moisen, G.G. 2011 Mapping wildfire and clearcut harvest disturbances in boreal forests with Landsat time series data. *Remote Sens. Environ.* **115**, 1421–1433.

Simard, M., Pinto, N., Fisher, J.B. and Baccini, A. 2011 Mapping forest canopy height globally with spaceborne lidar. *J. Geophys. Res. Biogeosciences* **116**, G04021.

Space, R.S., 1964. The Clearwater Story: A History of the Clearwater National Forest. Missoula: United States Department of Agriculture United States Forest Service Northern Region Office.

Spanner, M.A., Pierce, L.L., Peterson, D.L. and Running, S.W. 1990 Remote sensing of temperate coniferous forest leaf area index the influence of canopy closure, understory vegetation and background reflectance. *Int. J. Remote Sens.* **11**, 95–111.

Speer, J.H. 2010 *Fundamentals of Tree-ring Research*. University of Arizona Press.

Spies, T.A. 1998 Forest structure: A key to the ecosystem. *Northwest Sci.* **72**, 34–36.

Stage, A.R. 1976 An expression for the effect of aspect, slope, and habitat type on tree growth. *For. Sci.* **22**, 457–460.

Stage, A.R. and Crookston, N.L. 2007 Partitioning error components for accuracy-assessment of near-neighbor methods of imputation. *For. Sci.* **53**, 62–72.

Strobl, C., Boulesteix, A.-L., Kneib, T., Augustin, T. and Zeileis, A. 2008 Conditional variable importance for random forests. *BMC Bioinformatics* **9**, 307.

Tulbure, M.G., Wimberly, M.C., Boe, A. and Owens, V.N. 2012 Climatic and genetic controls of yields of switchgrass, a model bioenergy species. *Agric. Ecosyst. Environ.* **146**, 121–129.

Turner, D.P., Cohen, W.B., Kennedy, R.E., Fassnacht, K.S. and Briggs, J.M. 1999 Relationships between leaf area index and Landsat TM spectral vegetation indices across three temperate zone sites. *Remote Sens. Environ.* **70**, 52–68.

Turner, M.G. 2010 Disturbance and landscape dynamics in a changing world1. *Ecology* **91**, 2833–2849.

USDA, Forest Service, 2016. Forest Service Activity Tracking System (FACTs) harvest database. URL http://data.fs.usda.gov/geodata/edw/datasets.php. Acceded date 28/02/2018.

Varo-Martínez, M.Á., Navarro-Cerrillo, R.M., Hernández-Clemente, R. and Duque-Lazo, J. 2017 Semi-automated stand delineation in Mediterranean Pinus sylvestris plantations through segmentation of LiDAR data: The influence of pulse density. *Int. J. Appl. Earth Obs. Geoinformation* **56**, 54–64.

Vastaranta, M., Niemi, M., Wulder, M.A., White, J.C., Nurminen, K., Litkey, P., Honkavaara, E., Holopainen, M. and Hyyppä, J. 2016 Forest stand age classification using time series of photogrammetrically derived digital surface models. *Scand. J. For. Res.* **31**, 194–205.

Véga, C. and St-Onge, B. 2009 Mapping site index and age by linking a time series of canopy height models with growth curves. *For. Ecol. Manag.* **257**, 951–959.

Vogeler, J.C., Braaten, J.D., Slesak, R.A. and Falkowski, M.J. 2018 Extracting the full value of the Landsat archive: Inter-sensor harmonization for the mapping of Minnesota forest canopy cover (1973–2015). *Remote Sens. Environ.* **209**, 363–374.

White, J.C., Saarinen, N., Kankare, V., Wulder, M.A., Hermosilla, T., Coops, N.C., Pickell, P.D., Holopainen, M., Hyyppä, J. and Vastaranta, M. 2018 Confirmation of post-harvest spectral recovery from Landsat time series using measures of forest cover and height derived from airborne laser scanning data. *Remote Sens. Environ.* **216**, 262–275.

Wulder, M.A., Skakun, R.S., Kurz, W.A. and White, J.C. 2004 Estimating time since forest harvest using segmented Landsat ETM+ imagery. *Remote Sens. Environ.* **93**, 179–187.

Wulder, M.A., White, J.C., Loveland, T.R., Woodcock, C.E., Belward, A.S., Cohen, W.B., Fosnight, E.A., Shaw, J., Masek, J.G. and Roy, D.P. 2016 The global Landsat archive: Status, consolidation, and direction. *Remote Sens. Environ., Landsat 8 science results* **185**, 271–283.

Zhan, Q., Molenaar, M., Tempfli, K. and Shi, W. 2005 Quality assessment for geo-spatial objects derived from remotely sensed data. *Int. J. Remote Sens.* **26**, 2953–2974.

Zhang, C., Ju, W., Chen, J.M., Li, D., Wang, X., Fan, W., Li, M. and Zan, M. 2014 Mapping forest stand age in China using remotely sensed forest height and observation data. *J. Geophys. Res. Biogeosciences* **119**, 1163–1179.

Zimmerman, N., Presto, A.A., Kumar, S.P., Gu, J., Hauryliuk, A., Robinson, E.S., Robinson, A.L. and Subramanian, R. 2018 A machine learning calibration model using random forests to improve sensor performance for lower-cost air quality monitoring. *Atmospheric Meas. Tech.* **11**, 291–313.